AGU ADVANCING EARTH AND SPACE SCIENCE

Water Resources Research

RESEARCH ARTICLE

10.1029/2021WR031583

Key Points:

- New global-scale bedload and suspended bed material flux modules are introduced within the WBMsed framework
- Model performance and sensitivity analyses show strong correspondence to observations and dependence on discharge and river slope parameters
- The proportion of bedload flux is shown to be highly variable between and within basins, driven by topographic and hydrological settings

Supporting Information:

Supporting Information may be found in the online version of this article.

Correspondence to:

S. Cohen,
sagy.cohen@ua.edu

Citation:

Cohen, S., Syvitski, J., Ashely, T., Lammers, R., Fekete, B., & Li, H.-Y. (2022). Spatial trends and drivers of bedload and suspended sediment fluxes in global rivers. *Water Resources Research*, *58*, e2021WR031583. https://doi.org/10.1029/2021WR031583

Received 10 NOV 2021
Accepted 10 JUN 2022

Spatial Trends and Drivers of Bedload and Suspended Sediment Fluxes in Global Rivers

Sagy Cohen[1], Jaia Syvitski[2], Thomas Ashely[3], Roderick Lammers[4], Balazs Fekete[5], and Hong-Yi Li[6]

[1]Department of Geography, University of Alabama, Tuscaloosa, AL, USA, [2]CSDMS/INSTAAR, University of Colorado at Boulder, Boulder, CO, USA, [3]Civil and Environmental Engineering, Virginia Polytechnic Institute and State University, Blacksburg, VA, USA, [4]School of Engineering and Technology and Institute for Great Lakes Research, Central Michigan University, Mt. Pleasant, MI, USA, [5]Department of Civil Engineering, The City College of New York, City University of New York, New York, NY, USA, [6]Department of Civil and Environmental Engineering, University of Houston, Houston, TX, USA

Abstract Bedload is notoriously challenging to measure and model; its dynamics, therefore, remains largely unknown in most fluvial systems worldwide. We present results from a global scale bedload flux model as part of the WBMsed modeling framework that well predict the distribution of water discharge, suspended sediment and bedload. The sensitivity of bedload predictions to river slope, particle size, discharge, river width, and suspended sediment were analyzed, showing the model to be most responsive to spatial dynamics in river discharge and slope. The relationship between bedload and total sediment flux is analyzed globally, and for representative longitudinal river profiles (Amazon, Mississippi, and Lena Rivers). The results show that while the proportion of bedload decreases from headwaters to the coasts, there is considerable variability between basins and along river corridors. The topographic and hydrological longitudinal profiles of rivers are shown to be the key drivers of bedload trends, with fluctuations in slope controlling its more local dynamics. Estimates of water and sediment fluxes to global oceans from 2,067 largest river outlets (draining 67% of the global continental area) are provided. Estimated water discharge at 30,579 km^3/y corresponds well to past estimates; however, sediment flux is higher. Total global particulate load of 17.8 Gt/y is delivered to global oceans, 14.8 Gt/y as washload, 1.1 Gt/y as bedload, and 2.6 Gt/y as suspended bed material. The largest 25 rivers are predicted to transport more than half of the total sediment flux to global oceans.

Plain Language Summary Sediment carried by rivers varies considerably in space and time as a function of hydrological and environmental characteristics, and human-made modifications of river systems. Understanding and predicting the sediment dynamics within river systems are important, as they have direct impacts on the functioning of riverine and coastal ecosystems, water quality and use, and chemical dynamics of the Earth System as a whole (e.g., carbon fluxes). Sediment is transported in three modes: suspension for small particles, bedload for larger particles, and suspended bed material for medium particles. Bedload and suspended bed material are difficult to measure and model and thus remain largely unknown in most river systems. In this paper, we present new components to the WBMsed global hydro-geomorphic modeling framework that estimate bedload and suspended bed material fluxes for large rivers worldwide. We show good agreement with observations and provide an analysis of the distribution of the three sediment transport modes globally and, in greater detail, in three large river systems (Mississippi, Amazon, and Lena Rivers). An estimate of water and sediment fluxes to the global oceans is provided, the first to include all three sediment transport modes.

1. Introduction

Although quantifying Earth's fluvial sediment budget is important for fluvial and coastal geomorphology, ecology, flood analysis, and stream restoration (Best, 2019) there is a sevire scarcity in sediment monitoring worldwide (Syvitski et al., 2005), hindering advances in analysis and modeling. The total fluvial particulate load (Q_p) comprises of bedload (Q_b), suspended bed-material load (Q_{sbm}), and wash load (Q_w) (for definitions see Supporting Information S1) with the bedload portion being notoriously challenging to measure and model (Gomez, 1991; Kabir et al., 2012). Uncertainties in bedload measurements and modeling are particularly acute in large rivers (Ashley et al., 2020) and over large spatial domains (Lammers & Bledsoe, 2018). Use of acoustic sensing techniques for measuring bedload has increased in recent decades (e.g., Hackney et al., 2020; Nittrouer et al., 2008), providing high fidelity information in large rivers. However, the equipment cost, including deployment and technical expertise, limits the global reach of the methodology.

Modeling bedload can bridge the limited number of observations and offer an analytical framework for scientific studies and predictions. Bedload formulas range from simplified approximations (e.g., Meyer-Peter & Müller, 1948; Parker, 1990) to complex physically-based numerical models (e.g., Coulthard et al., 2013; Kabir et al., 2012; Schmitt et al., 2016). HydroTrend v.3.0 (Kettner & Syvitski, 2008), a basin outlet model, implemented a modified version of the Bagnold (1966) bedload flux equation that, like the equation used in the present study, is a simplified stream-power model. The modified Bagnold (1966) equation (initially proposed in Syvitski & Saito, 2007) is attractive for large-scale modeling as it simplifies stream-power calculations into only two dynamic parameters (water discharge and river slope), assuming a uniform sandy riverbed. No evaluation of the equation has been reported. The Hatono and Yoshimura (2020) global sediment model employs a detailed stream-power/shear-velocity equation to calculate bedload using river width, sediment particle diameter, shear velocity, critical shear velocity, critical shear stress, and suspending velocity parameters. Hatono and Yoshimura (2020) demonstrated that suspended sediment predictions of their model correspond well to observations, but offered no analysis concerning the performance of the bedload flux predictions. Moreover, the shear parameters in their bedload equation are very challenging to simulate and evaluate, especially for coarse resolution simulation. MOSART-sediment (H.-Y. Li et al., 2022) is a newly developed large-scale sediment model utilizing a continuous map of median bed-material sediment particle diameter over the contiguous U.S. (Abeshu et al., 2021), with river slope values derived from the NHDplus database (McKay et al., 2012) and other parameters estimated a priori. H.-Y. Li et al. (2022) invoke the classic Engelund-Hansen equation (Engelund & Hansen, 1967) to simulate the total bed-material load and a new empirical formula to separate the total bed-material load into bedload and suspended bed-material load. H.-Y. Li et al. (2022) also do not provide an estimate of MOSART-sediment bedload predictions.

Despite a rich research history, large-scale predictions of bedload flux remain elusive (Gomez, 1991; Kabir et al., 2012), given the reliance of these equations on local conditions such as shear stress and near-bed velocity parameters, which are difficult to simulate (Lammers & Bledsoe, 2018). Several recently proposed bedload equations include simplified approximations of near-bed hydraulic parameters that can be easily obtained or predicted (i.e., Ashley et al., 2020; Lammers & Bledsoe, 2018; Syvitski & Saito, 2007). Here we present new bedload and suspended bed material modules within the WBMsed global hydrogeomorphic framework (Cohen et al., 2013, 2014). In this study, we use the Lammers and Bledsoe (2018) bedload equation and the Syvitski et al. (2019) suspended bed material equation, along with WBMsed existing suspended sediment module, to analyze and map the spatial dynamics of bedload in the context of the total fluvial sediment budget at a global scale. We introduce novel global-scale estimates of bed particle size, river slope, and water density (model parameters). We offer details on three rivers (Amazon, Mississippi, and Lena) as case studies for understanding longitudinal dynamics and an analysis of sediment flux to global oceans from 2,067 river outlets.

2. Methodology

2.1. Modeling Framework

2.1.1. Hydrological Engine

WBMsed is an open-source modular global scale hydrogeomorphic model (Cohen et al., 2013), an extension of the WBMplus global hydrology model (Wisser et al., 2010), part of the FrAMES biogeochemical modeling framework (Wollheim et al., 2008). WBMplus simulates water balance/transport at a daily time step as a function of gridded climatic inputs, soil moisture balance, runoff generation mechanisms, and transport. WBMplus is unique in the number and explicitness of anthropogenic factors: dam operation, irrigation (water uptake from rivers, reservoirs, groundwater), and agriculture (impacting evapotranspiration). WBMsed sediment modules use discharge and water temperature, simulated respectively by WBMplus and WBM-TP2M (see Miara et al., 2018; Syvitski et al., 2019) modules within FrAMES.

2.1.2. Suspended Sediment Module

WBMsed employs the *BQART* model (Syvitski & Milliman, 2007) as the governing suspended sediment flux equation. BQART calculates the long term-average suspended sediment load in kg/s ($\overline{Q}_s = \omega B\ \overline{Q}^{0.31} A^{-0.5} RT$)

based on average water discharge ($\overline{Q}$), runoff contributing *A*rea, maximum topographic *R*elief, averaged ground surface *T*emperature, and a catchment parameter ($B = IL(1 - T_e)E_h$) that incorporates a glacial erosion factor (I), *L*ithology factor, trapping efficiency of catchment reservoirs (T_e), and a human-influenced erosion factor (E_h). BQART is calculated for each grid cell as a function of these upstream basin characteristics with the temporally dynamic parameters updated during the simulation from initial spin-up values. Daily Q_s predictions are calculated using the Psi equation (Morehead et al., 2003) which provide a spatially explicit power-law rating curve based on the relationship between daily and average discharge (Q and $\overline{Q}$ respectively) in each grid-cell. Detailed description and analysis of WBMsed suspended sediment module are provided in Cohen et al. (2013, 2014).

2.1.3. Bedload Module

The WBMsed module is written to allow developers to easily add alternate bedload algorithms, and for users to select amongst these from the model simulation's script. Currently, the WBMsed bedload module includes the Lammers and Bledsoe (2018) equation, modified Bagnold (1966) equation (following Kettner and Syvitski (2008)), and an empirical equation proposed by Ashley et al. (2020). The Lammers and Bledsoe (2018) equation is employed for this study given that its simplified parameterization of stream power is well suited to large-scale modeling and given that it was extensively evaluated and compared against other bedload equations (Lammers & Bledsoe, 2018). In WBMsed, the Lammers and Bledsoe (2018) equation was modified from its original per-unit width bedload transport rate (kg/m/s) to bedload flux, Q_b (kg/s):

$$Q_b = \left[a(\omega - \omega_c)^{1.5} D_s^{-0.5} \left(\frac{Q}{w} \right)^{-0.5} \right] w\,; \text{when}\, \omega > \omega_c \tag{1}$$

where a is a coefficient (1.4×10^{-4}) (−), D_s is representative grain size (m), Q is discharge (m^3/s), and w is river width (m), ω and ω_c are specific and critical stream powers (W/m^2):

$$\omega = \frac{\rho g Q S}{w} \tag{2}$$

$$\omega_c = 0.1\rho[(s-1)gD_s]^{1.5} \tag{3}$$

where ρ is fluid density (kg/m^3), g is the acceleration due to gravity (constant 9.8 m/s^2), S is river slope (m/m), and s is a unitless sediment-specific gravity (assumed to be 2.65). w and D_s are estimated using empirical expressions derived from databases reported by Ma et al. (2017) and Recking (2019). Taken together, these comprise 13,000+ observations of relevant parameters from 56 different rivers with $\overline{Q} > 30$ m^3/s, spanning four orders of magnitude of grain size (40 μm to 20 cm) and a factor of ∼40 in river width (22–900 m). Width and grain size relations are derived using mean values for each river. The width relation ($R^2 = 0.71$) is given by:

$$w = 2.15\overline{Q}^{0.67} \tag{4}$$

This expression is purely empirical but captures a strong first-order trend that is robust for large rivers ($Q > 30$ m^3/s). Considering additional predictor variables does not improve predictive power and the results are consistent with the data set compiled by Dunne and Jerolmack (2018), using 37 rivers with width between 500 and 3,400 m. The grain size relation ($R^2 = 0.9$) is given by:

$$D_s = 3.77\left(\frac{\overline{Q}}{W} \right)^{1.42} S^{1.26} \left(\frac{\overline{Q_S}}{W} \right)^{-0.5} \tag{5}$$

The form of this expression may be derived from dimensional considerations per the arguments presented in Ashley et al. (2020).

WBMsed simulates daily water density, ρ, as a function of fluid temperature (T_w, °C) calculated using the Thiesen-Scheel-Disselhorst equation (McCutcheon et al., 1993):

$$\rho = 1000 \left[\frac{1 - (T_w + 288.94)}{508929.2\,(T_w + 68.12)} \right] (T_w - 3.98)^2 \tag{6}$$

Q_b is calculated in each grid-cell and time step as a function of updated parameter values. Cell-to-cell Q_b transport is not simulated. Upstream and temporal dynamics are driven by variability in Q, Q_s, and T_w, making Q_b transport limited, similar to the assumptions made in H.-Y. Li et al. (2022). We discuss this assumption in Section 4.

2.1.4. Suspended Bed Material Module

Suspended bed-material flux (SBM; Q_{sbm}; kg/s) is calculated following Syvitski et al. (2019):

$$Q_{sbm} = \left(\frac{\rho_s}{\rho_s - \rho}\right) \rho Q^{\beta} S \left(0.01 \frac{\mu}{\mu_s}\right) \tag{7}$$

where ρ_s is sediment density (assumed 2,650 kg/m^3), μ and μ_s are flow and settling velocities (m/s) respectfully, and β is a bedload rating term (here assumed 1.0). Transport velocity is simulated by the model as a function of channel geometry and discharge (i.e., Manning's equation). Settling velocity is calculated as a function of kinematic viscosity ($f[D_s, T_w, \rho_s, \rho]$), D_s, ρ_s and ρ. In this study, Q_{sbm} is used to calculate the wash load as $Q_w = Q_s - Q_{sbm}$.

2.2. Simulations Setup, Inputs, and Postprocessing

Gridded global-scale simulations are conducted at 6 arc-minutes (0.1 degree) spatial resolution (~11 × 11 km at the equator) and daily time steps between 1960 and 2019. The first 30 years of the simulations (1960–1989) are used as spin-up and thus excluded from the analysis. Simulations are made in the model's "disturbed" mode wherein all the anthropogenic processes are included for both the hydrological engine (irrigation, dam flow regulation, water uptake, agriculture evapotranspiration) and suspended sediment module (T_e and E_h). The Q_b and Q_{sbm} modules do not include direct anthropogenic parameters except through modifications to Q and Q_s. The potential significance of this is discussed later.

The model input datasets are detailed in Cohen et al. (2013); alterations include: precipitation - monthly TerraClimate (Abatzoglou et al., 2018) data set re-gridded at 10 arc-minutes resolution, partitioned into daily data by computing the daily fraction from the NCEP reanalysis product (Kalnay et al., 1996; Kistler et al., 2001); air temperature - monthly TerraClimate (Abatzoglou et al., 2018) data set re-gridded at 10 arc-minutes resolution; reservoir capacity—global reservoir and dam database (GRanD v1.3; Lehner et al., 2011); and flow network—6 arc-minute HydroSTN30 network which is a derivative from HydroSHEDS high resolution gridded network from Lehner et al. (2008).

River slope was originally rasterized from the Lin et al. (2020) global river width data set that employed the 90 m resolution MERIT Digital Elevation Model (DEM) to estimate channel slope along flow paths. Lin et al. (2020) was selected over the GloRS data set (Cohen et al., 2018) given its calculated values in coastal reaches (GloRS mostly include a constant minimum value for these very low hydrological slopes). The Lin et al. (2020) data set exhibits a high degree of noise, expressed as high levels of fluctuations along river paths (see Figure S1 in Supporting Information S1 for the Mississippi/Missouri longitudinal profile). These fluctuations are not realistic. To alleviate this issue, a smoothed river slope raster was generated by "burning" the 25th percentile slope value extracted for each WBMsed stream network reach into the global river slope input layer (maximum length 200 km). Figure S1 in Supporting Information S1 shows a comparison between the smoothed and original datasets.

Long-term average model predictions are calculated between 1990 and 2019 for all the analyzed parameters. The analysis presented in the present paper only includes grid-cells with an average discharge greater than 30 m^3/s (total ~10^5 grid-cells). Masking of grid-cells with $Q < 30$ m^3/s reduces known model and input data biases in streams and small rivers and focuses our analysis on reaches of medium to large rivers. A vectorized version of the model's stream network is used for visualization.

2.3. Model Evaluation

Three datasets are used to evaluate the model's average Q, Q_s, and Q_b predictions. Q and Q_s are compared against (a) average observations in 39 USGS sites where the discharge record is over 20 years (Table S1 in Supporting Information S1), and (b) estimated values reported in 132 global basin outlets from the M&S05 database (Syvitski

& Milliman, 2007). Q_b and Q_{sbm} are compared to a subset of bedload observations compiled by Islam (2018). Given that these bedload observations are not based on continuous monitoring, but rather on limited sporadic sampling, comparison to average bedload predictions is problematic. We, therefore, use this analysis mainly to gain a general evaluation of the model implementation within WBMsed. Q_b observations were included in the analysis if the difference between the reported and predicted water discharge for a given record was less than 80%. Subsetting based on differences in Q reduces biases in the analysis stemming from location errors and differences in temporal averaging and flow conditions (e.g., observations are from predominantly high flow conditions). An 80% threshold is quite high (inclusive) but given the small size of the database, it was a compromise used in order to maintain a sizable subset. The subset includes 24 out of 44 sites and has a range of 3+ orders of magnitude in average Q and Q_b (Table S2 in Supporting Information S1).

3. Results

3.1. Model Evaluation

Model Q and Q_s predictions are strongly correlated (log-log linear), with R^2 of 0.99 and 0.89 respectively (Figure S2 in Supporting Information S1; Q_s data ranges 3+ orders of magnitudes), at the 39 USGS sites. Strong correspondence is also found to the M&S05 database, with an $R^2 = 0.99$ for Q and 0.73 for Q_s (Figure S3 in Supporting Information S1; Q_s data ranges 4+ orders of magnitudes). WBMsed underpredicts Q compared to both datasets; by 57% for the USGS data set (Table S1 in Supporting Information S1) and 12% for M&S05. Note that the timeframe of each observation point differs and, for most gage sites, covers only part of the modeled 1990–2019 timeframe. Q_s is slightly (5%) underpredicted compared to the USGS data, but considerably overpredicted (60%) compared to the M&S05 datasets, mainly due to considerable overprediction in the Amazon River (described later).

Overall, results show the robustness of WBMsed at predicting Q and Q_s for global rivers, and improvement of the model's current version (stronger validation results when compared to its most recent analyses in Dunn et al. (2018, 2019) and Moragoda and Cohen (2020)). The improvement in the model is due to an increase in accuracy of its hydrological predictions, attributed to recent enhancements to the WBMplus framework, use of higher resolution precipitation data set (TerraClimate), and enhancements in the WBMsed Q_s trapping module (including updating the reservoir input to the latest GRanD (v1.3) data set).

Lammers and Bledsoe (2018) conducted an extensive evaluation of their bedload model against a large data set of field and flume data and found strong correspondence ($R^2 = 0.75$), particularly in the sand fraction (the smallest fraction in their analysis; cf. Figure 4 in Lammers & Bledsoe, 2018). Field data used in Lammers and Bledsoe (2018) is almost exclusively from small rivers and creeks. Thus, when implemented in WBMsed, the predictive quality of their bedload model, cannot be readily assumed from their study to the present study, given its global resolution, temporal averaging, and dominant bed particle size. Our comparison between observed and predicted Q_b shows good agreement ($R^2 = 0.83$; Figure 1) and is similar in shape (relative to a 1:1 line) to the results of Lammers and Bledsoe (2018). The model predicts an average of 45.4 kg/s for this data set compared to 79.6 kg/s for the observed data (Table S2 in Supporting Information S1). The model overpredicts low values (<3 kg/s) by over an order of magnitude in some cases, while maintaining a fairly tight distribution around (mostly below) the 1:1 line for mid and high Q_b values.

Predicted Q_{sbm} yields a reasonable regression ($R^2 = 0.81$; Figure S2 in Supporting Information S1) when compared to the Q_b observations and a higher overall average (141 kg/s). Regression between predicted Q_b and predicted Q_{sbm} in the 24 locations is strong ($R^2 = 0.89$), explained by the mechanistic similarity and connectivity between Q_b and Q_{sbm}, particularly for sand-bed rivers. A strong co-dependence exists between Q_b and Q_{sbm}, especially when temporally averaged, and the two equations share several forcing parameters (S, Q, ρ, D_s).

3.2. Sensitivity of Bedload Predictions to Key Parameters

Lammers and Bledsoe (2018) conducted a sensitivity analysis of their bedload equation and found that the Q and S have the highest sensitivity index (0.25 and 0.2 respectively), followed by w and D_s (~0.1), and ω_c (<0.05). These sensitivity values reflect the Q_b equation formulation and the distribution and uncertainty in the input data. For WBMsed, the sensitivity of the results to key parameters can be assumed to differ from the results of

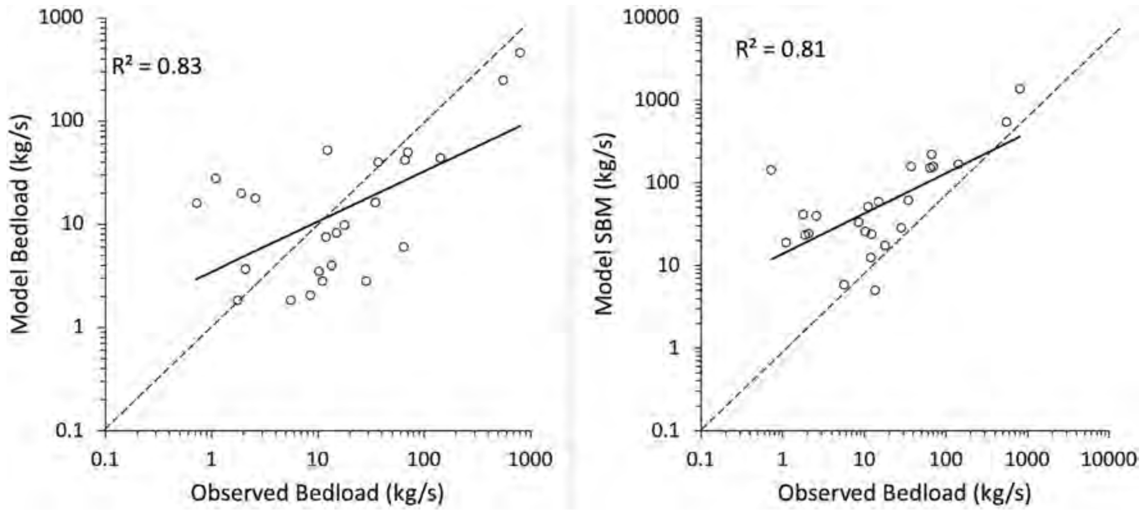

Figure 1. Predicted versus observed (a) bedload (Q_b) and (b) suspended bed-material (Q_{sbm}), both against observed bedload. The dashed line is the 1:1 line; the solid line is the best fit log-log linear (power-law) regression.

Lammers and Bledsoe's (2018), given differences in input data and the temporal explicitness (daily) of the simulations. The latter, in particular, merit reanalysis of the model sensitivity given Equation 1 $\omega > \omega_c$ daily conditioning. Simply put, average predictions of the model are reflective of the mathematical relationships between Q_b and its predictive parameters as well as the spatial and temporal dynamics in the input data and simulated flow conditions. The sensitivity of the WBMsed global average Q_b predictions was conducted by calculating the regression between predicted Q_b and S, Q, w, and D_s for 91,659 grid-cells (with $Q > 30$ m^3/s and $Q_b > 1$ kg/s). Parameter magnitudes were normalized between 0 and 1 to allow for direct comparison, using log-log linear regression due to data skewness.

Results (Figure 2) show Q_b to be strongly affected by Q, closely followed by S and w. Model Q_b predictions are least sensitive to D_s. These results are similar to Lammers and Bledsoe (2018), though here the differences in the sensitivity of Q_b to the four parameters are quite small. The relatively high sensitivity to D_s and S increases uncertainty in the bedload predictions as these two parameters are the most challenging parameters to estimate/calculate. River slope calculations are highly sensitive to the accuracy and resolution of the DEM used, and the spatial alignment between the DEM and the stream network (Cohen et al., 2018). Particle size is challenging to estimate and represent in a single parameter given its often high spatial variability and actual value distribution within a single sample. Here D_s is considered as a median riverbed particle size (D_{50}).

3.3. Spatial Dynamics and Relationships

Bedload distribution (Figure 3) is highly heterogeneous globally, across basins and along main river corridors. High bedload values are prominent in larger rivers and mountainous (headwater) reaches (primarily Himalaya). This duality in bedload distribution stems from the two core drivers of stream power: increasing discharge downstream contrasts with river slope that generally decreases downstream (Figure 4). Slope and discharge, therefore, limit each other at an intra-basin scale. Much of the local spatial variability is attributed to particle size and river slope due to their strong effect on bedload.

The relationship between Q_b and Q_s is also complex. The relationship at a pixel-to-pixel comparison is weak ($R^2 = 0.47$; Figure S4 in Supporting Information S1). Q_s values are strongly influenced by upstream basin area and have a strong increasing trend in the downstream direction (except for trapping behind dams). This leads to contrasting trends with bedload in some locations. Given the complexity in Q_b distribution, latitudinally-averaged values (Figure 5b) show limited variability (<1 order of magnitude) compared to Q_s (>3 orders of magnitude; Figure 5c) with large tropical and mid-latitude rivers dominating the global sediment flux patterns (Figure 3).

Globally averaged statistics (grid-cells with $Q > 30$ m^3/s) (Table 1) quantify the considerable variability in sediment flux and forcing parameters. For both Q_b and Q_s, the planetary standard deviation greatly exceeds both its

10.1029/2021WR031583

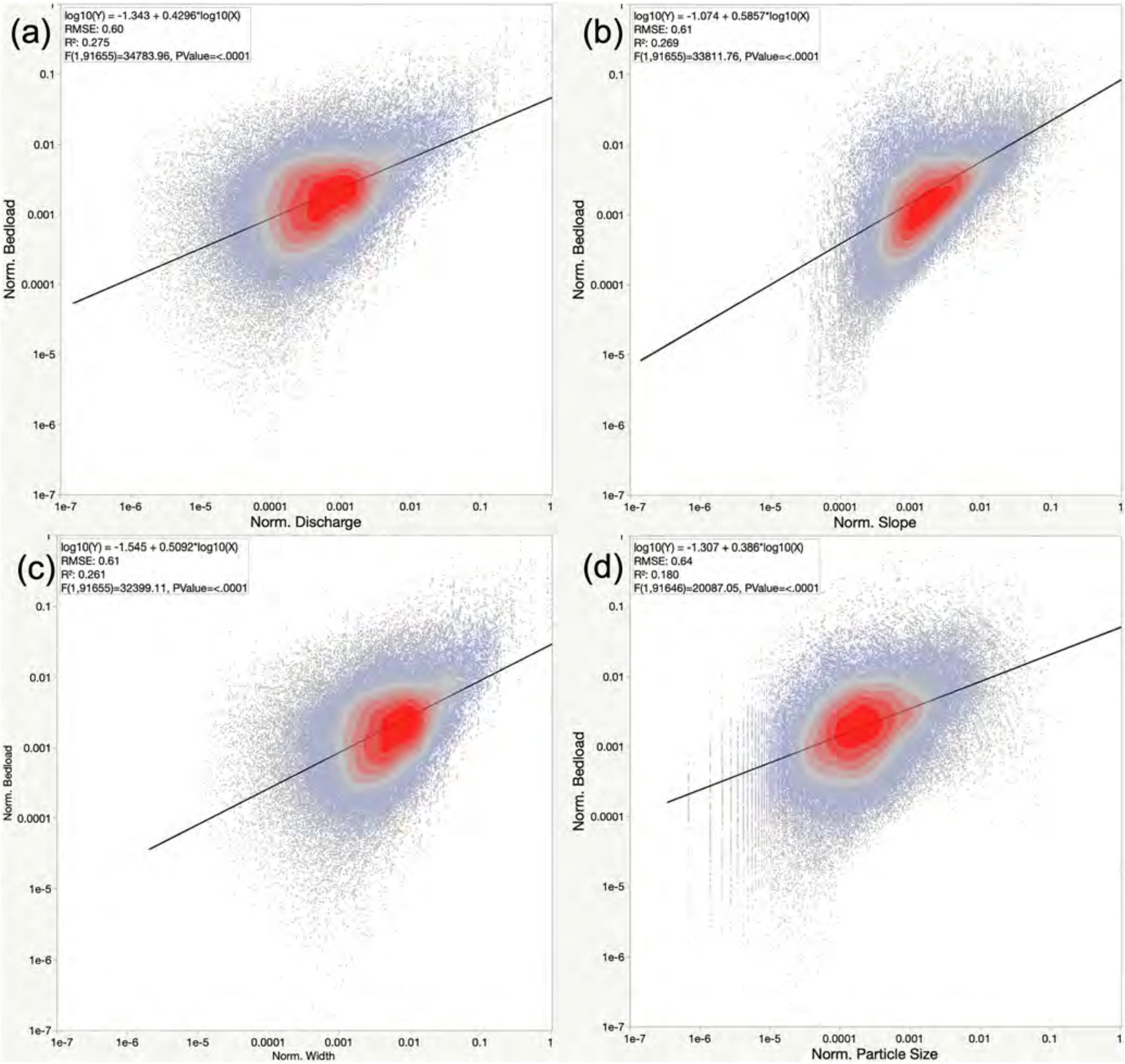

Figure 2. WBMsed model sensitivity plots showing the regression between normalized [0,1] bedload at the modeled domain (91,659 grid-cells) and (a) discharge, (b) river slope, (c) river width, and (d) particle size.

mean and especially its median values (Table 1). This further demonstrates the challenges in bedload predictions, but also the utility in model simulations that allow for relationship discovery between drivers and other fluvial and environmental factors.

The proportion of bedload from the total sediment flux ($Q_t = Q_b + Q_s$) is low (<2.5%) for large tropical and mid-latitude rivers (Figure 5a). In high latitudes (>50°), bedload proportion is high (Figure 5d), particularly in small and mid-size rivers (Figure 5a). This latitudinal trend is driven by low Q_s magnitudes in colder river basins, rather than higher bedload magnitudes (Figures 3, 5b, and 5c). Averaged globally, the model proportion of bedload appears high (mean of 24% and median of 15%; Table 1) compared to historical land-sea (coastal) estimates (10% Meade et al., 1990; 6.5% Syvitski & Saito, 2007). This is explained by the fact that smaller rivers are not weighted by discharge for these statistics and, thus, skew the results. Babiński (2005) cataloged the considerable variability in bedload proportion, disputing the commonly referenced range of 1%–15%, showing

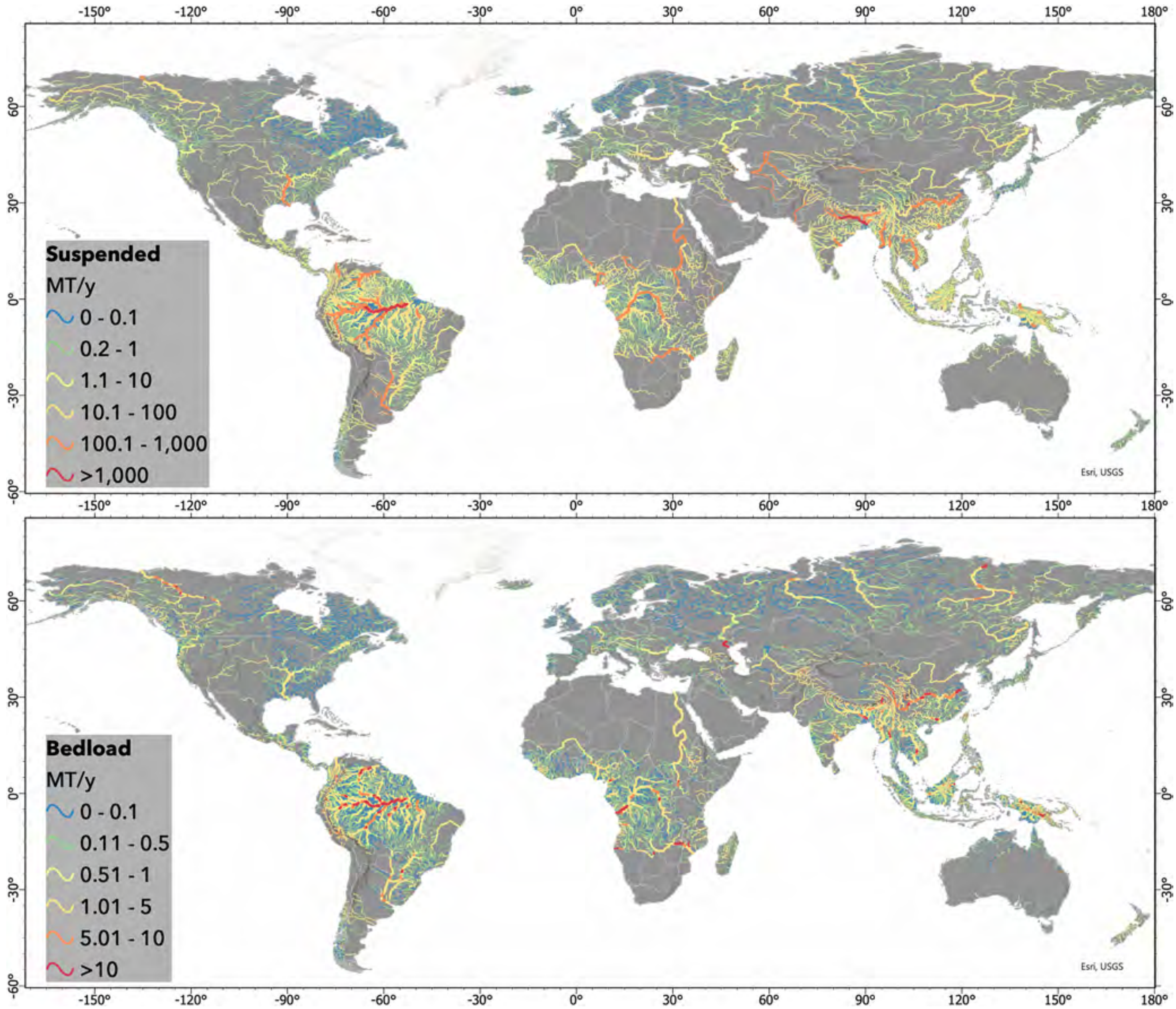

Figure 3. Average (1990–2019) predicted Q_s (top) and Q_b (bottom) in Mt/y. The width of the lines is indicative of average river-reach discharge. Note differences in color scheme scale. A link for an interactive Web-GIS portal (ArcGIS Online Map Viewer) for these maps and the other global maps presented in this paper is provided in the "Data Availability Statement" section.

a Q_b/Q_s ratio ranging from 0.3% to 87% in 14 large rivers in Russia and China. Our results show a median Q_b/Q_s ratio of 0.2 (20%), with a high mean and standard deviation (Table 1), driven by the dominance of small river cells in this analysis.

3.4. River Outlets

The proportion of bedload at river outlets decreases in larger rivers but with considerable variability (note outliers in Figure 6). Regression between bedload proportion and Q is weak ($R^2 = 0.16$). Once smaller rivers are filtered out for a discharge-segregated outlet analysis, bedload proportion decreases considerably (Figure 6; Table 2). When considering river outlets with $Q > 100$ m^3/s, thus eliminating more than 50% of river mouths (from 2,067 to 919 outlets), Q_b proportion is reduced to a median of 11% (mean 21%) from 22% (mean 32%). The average bedload proportion is 11% for medium rivers ($Q > 500$ m^3/s) and 5.3% for large rivers ($Q > 2,500$ m^3/s), in line with the model estimates of 6.5% by Syvitski and Saito (2007).

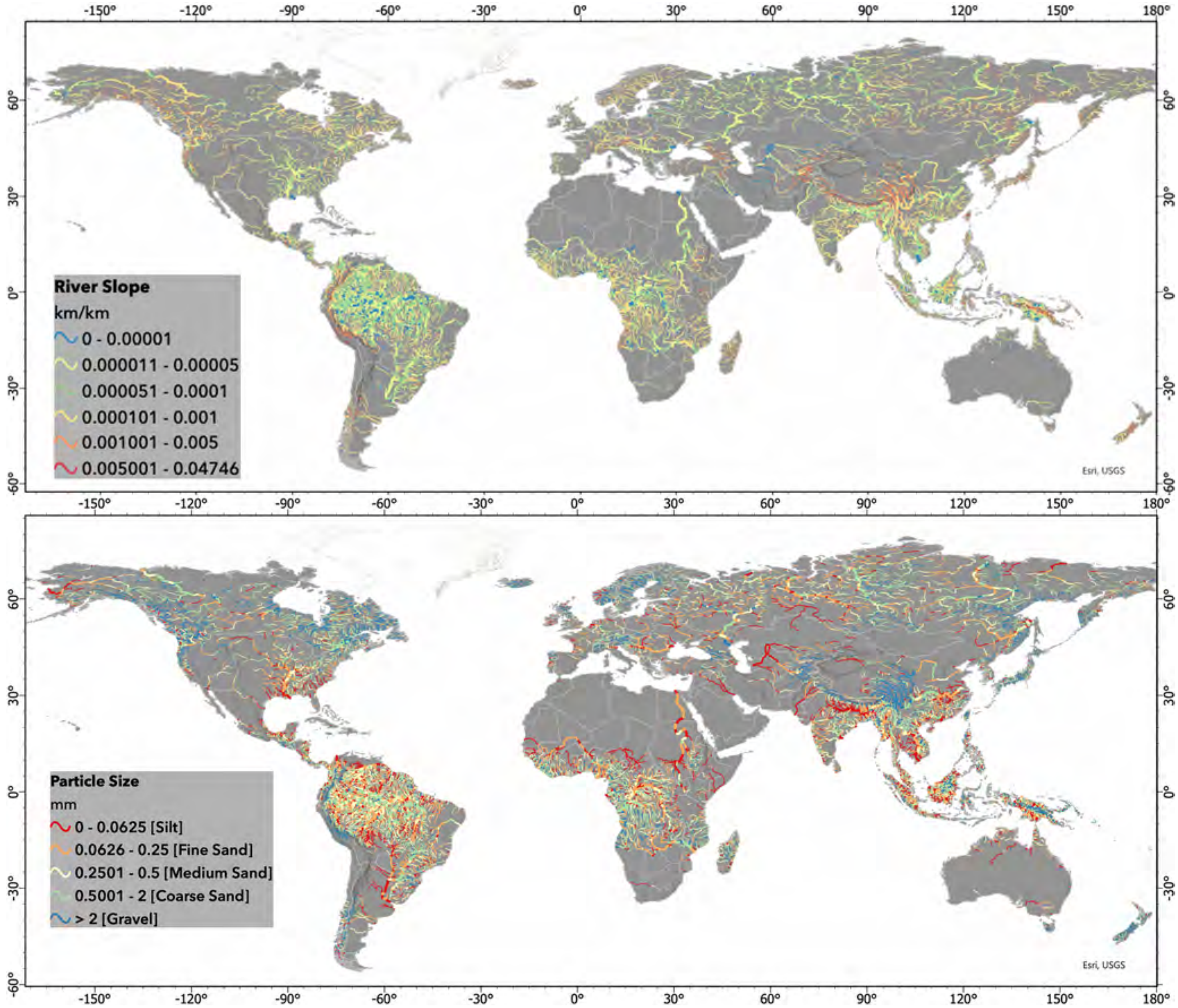

Figure 4. River slope (top) and particle size (bottom) maps. The width of the lines indicates average river-reach discharge.

L. Li et al. (2020) provide a recent estimate of Q and Q_s flux to global oceans based on new data and the Milliman and Farnsworth (2011) data set. Their estimate, based on 1,232 rivers for Q and 769 for Q_s, is 31,629 km^3/y and 12,890 MT/y, respectively, similar to previous estimates. Our predicted Q (for all 2,067 analyzed outlets where $Q > 30$ m^3/s); draining 68% of the continental landmass (excluding Antarctica)), also correspond to the L. Li et al. (2020) value (30,579 km^3/y; Table 2). Our results further show that half of the water discharge to global oceans is from the 25 largest global rivers ($Q > 5{,}000$ m^3/s; draining 33% of continental landmass).

The two rivers with the greatest suspended sediment flux, the Amazon and Ganges-Brahmaputra, were grossly overpredicted (by a factor of 8 and 2 respectively) compared to the most recent published estimates (Montanher et al. (2018) for the Amazon and Syvitski et al. (2022) for the Ganges-Brahmaputra). It should be noted that, for both rivers, estimates of sediment flux to the ocean vary considerably in the literature (Montanher et al., 2018; Rahman et al., 2018; Syvitski et al., 2022). Given the importance of these two rivers for the calculation of suspended sediment flux to global oceans, the sum of suspended, washload, and total sediment fluxes (in MT/y; left-most column in Table 2; values denoted with 'a') were adjusted by using 720 and 1,894 MT/y for the Amazon and Ganges-Brahmaputra respectively based on Montanher et al. (2018) and Syvitski et al. (2022). Calculated bedload proportion and bedload/suspended are based on the updated values (right-most column in Table 2).

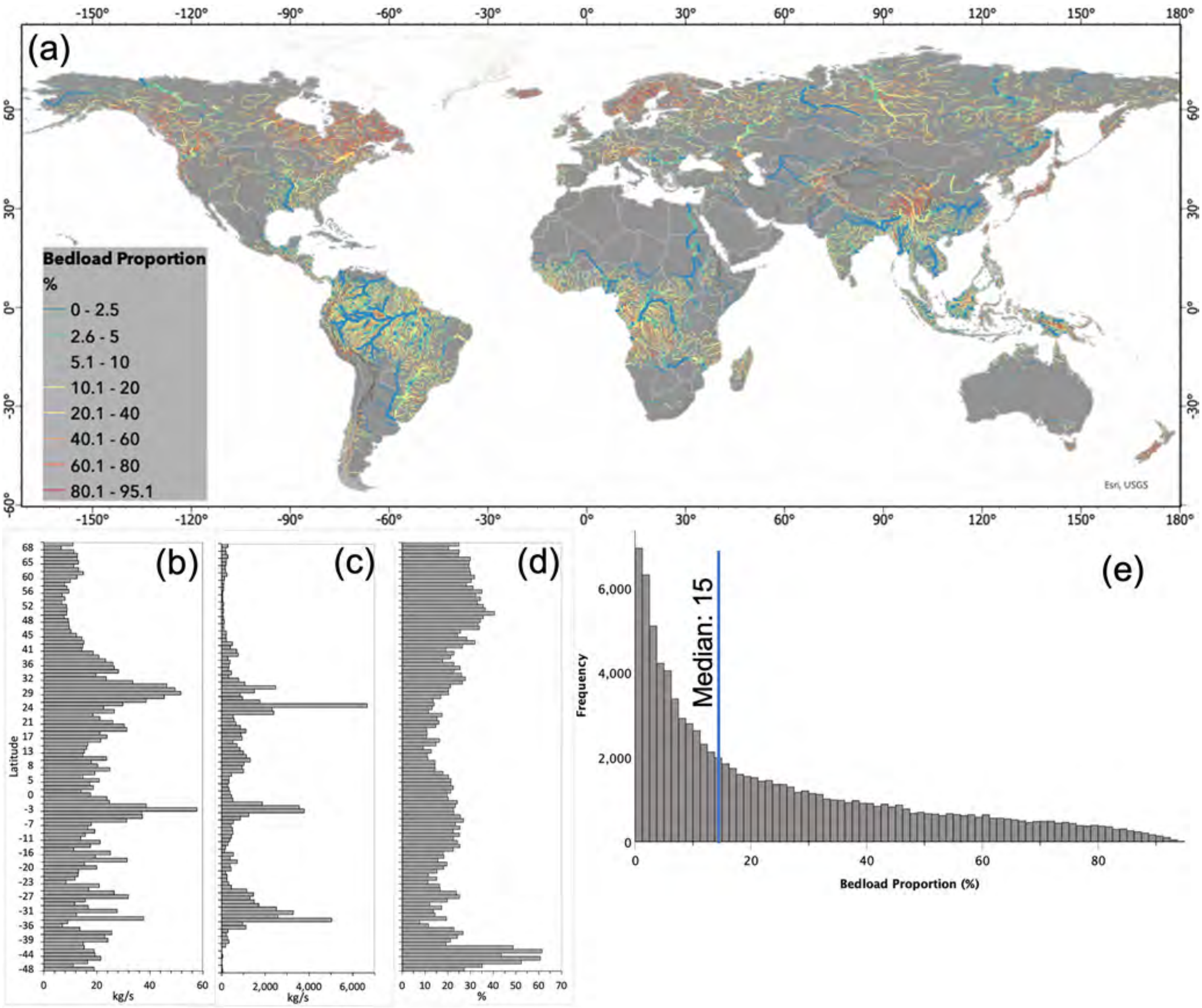

Figure 5. The proportion of bedload flux from total sediment flux (a) map, (b) bedload latitudinal averages, (c) suspended load latitudinal averages, (d) bedload proportion latitudinal averages, and (e) histogram of all grid cells ($Q > 30$ m^3/s).

After adjusting for the Amazon and Ganges-Brahmaputra, our Q_s estimate for all analyzed outlets is 25% higher than L. Li et al. (2020), with a predicted Q_s of 16,636 MT/y. Q_s predictions for the 919 outlets with $Q > 100$ m^3/s, more closely corresponding to the number of outlets used in L. Li et al. (2020) (769), is 15,146 MT/y. For the top 218, river outlets ($Q > 500$ m^3/s) predicted Q_s is 12,223 MT/y, which closely corresponds to L. Li et al. (2020). The sum of the model predicted Q_s for the 39 USGS gages used for validation (Section 3.1) is lower than observed Q_s (17,790 and 16,892 kg/s for predicted and observed respectively) but are overpredicted for the 128 observations in the M&F05 database (283,509 and 153,376 kg/s for predicted and observed respectively without adjusting for Amazon and Ganges-Brahmaputra). The M&S07 database includes many outdated and partial data, some of which were reused in the Milliman and Farnsworth (2011) database. Given that our predictions (a) correspond well and underpredict USGS observations, (b) are based on nearly 3 times more outlets (2,067 vs. 769), (c) still only represents 68% of Earth's landmass, and (d) underpredict Q, we assert that our new estimate of total sediment flux to global oceans is likely more robust and may even be conservative. Our results do not include Greenland, which was estimated to have an additional Q_s flux of >1 Gt/y (Overeem et al., 2017). Our predictions, however, likely underestimate sediment trapping due to the limited number of dams represented (~7,000 large dams compared to ~60,000 reported dams; ICOLD database 2017).

Table 1
Summary Statistics for All Grid-Cells With $Q > 30$ m³/s, $Q_b > 1$ kg/s ($N = 91,659$)

	Mean	Median	Std. deviation
Discharge [m³/s] (km³/y)	960 (30)	121 (3.8)	5679 (179)
Suspended [kg/s] (Mt/y)	657 (20)	30 (0.9)	4169 (131)
Bedload [kg/s] (Mt/y)	19 (0.6)	5 (0.15)	55 (1.7)
Suspended bed-material [kg/s] (Mt/y)	64 (2)	24 (0.7)	149 (4.7)
Wash load [kg/s] (Mt/y)	602 (19)	8 (0.2)	4075 (128)
Total sediment load [kg/s] (Mt/y)	676 (21)	41(1)	4195 (132)
Bedload proportion [%]	24	15	23
Bedload: suspended load	0.6	0.2	1.2
River slope [km/km]	0.0003	0.0001	0.001
Bed-material particle size [mm]	1.4	0.2	7.8

Bedload flux to global oceans is estimated at 1.1 Gt/y (1145 Mt/y; Table 2). Nearly half of the estimated Q_b is from smaller rivers ($30 < Q < 100$ m³/s; 1,148 out of 2,067 analyzed outlets). Bedload flux from the top 25 largest rivers ($Q > 5,000$ m³/s) is only 111 Mt/y (<10% of the total flux). These contrasting results from Q_s are due to the much lower river slope in large rivers (by over an order of magnitude) compared to all other outlets (Table 2). Median particle size is relatively consistent for all river size classes (Table 2). The bedload proportion distribution among global outlets (Figure 7), shows high values in outlets in high latitudes and islands (e.g., Japan, New Zealand, equatorial pacific islands). The former, as discussed earlier, can be explained by lower suspended sediment in colder regions, while the latter can be attributed to high river slopes in mountainous islands.

Total sediment flux ($Q_s + Q_b$) to global oceans is predicted here to be 17.7 Gt/y (17,780 Mt/y) for all analyzed outlets. The 25 largest rivers contribute nearly half, with a total sediment flux of 8,282 MT/y, driven by Q_s. Washload (Q_s—Q_{sbm}) to global oceans is predicted to be 14.6 Gt/y (14,683 MT/y) with the 25 largest rivers contributing over 50%, with a total washload sediment flux of 7,758 Mt/y.

The proportion of bedload in global sediment flux to global oceans is calculated in Table 2 (right-most column) as the ratio between the sum of Q_t and Q_b in each bracket. This calculation differs from the mean, median, and standard deviation reported in Table 2 and Figure 6 as these are raw bedload proportion statistics for all the outlets in each bracket, not taking into account the relative amount of sediment in each (i.e., an outlet for a small river is equally weighted). The calculated proportion of bedload for all analyzed outlets is 6.4%. Larger rivers have a considerably lower bedload proportion, with the largest 25 rivers having a value of 1.3%.

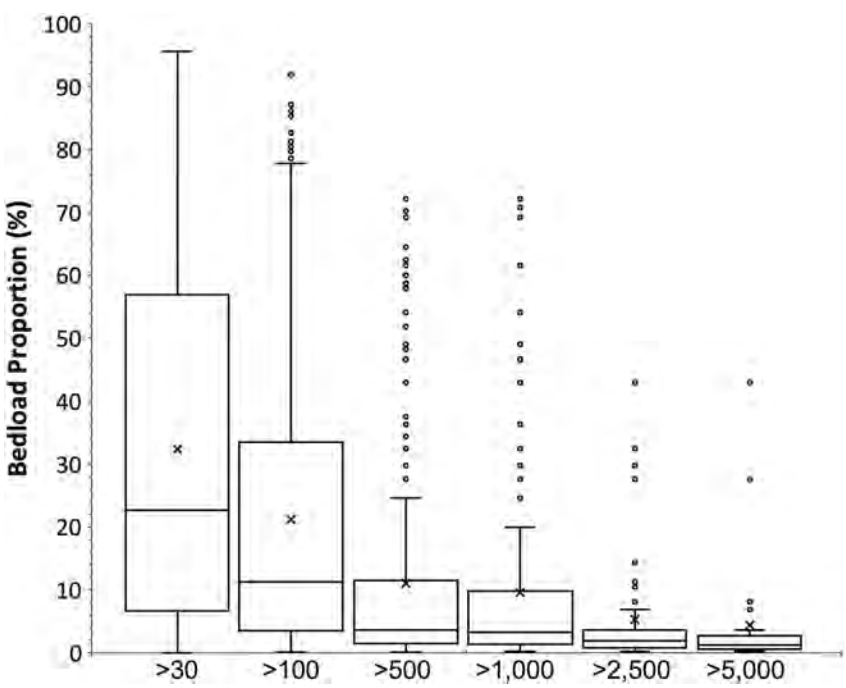

Figure 6. Boxplots of bedload proportion in river outlets to global oceans, with average discharge greater than 30 m³/s ($n = 2,067$, draining 67% of continental land mass (excluding Antarctica)), 100 m³/s ($n = 919$, draining 60%), 500 m³/s ($n = 218$, draining 50%), 1,000 m³/s ($n = 114$, draining 44%), 2,500 m³/s ($n = 47$, draining 37%), and 5,000 m³/s ($n = 25$, draining 33%). Black line within each box denotes the median, x denotes the mean and circles are outliers.

Table 2
Statistics for River Outlets at 6 Discharge Filtering Brackets

	Outlet filter (m^3/s)	Mean	Median	Standard deviation	Sum (m^3/s) or (kg/s)	Sum (km^3/y) or (MT/y)
Discharge (m^3/s)	>30	466	84	4,387	964,342	30,579
	>100	979	234	6,547	900,025	28,540
	>500	3429	1043	13,169	747,703	23,710
	>1000	5912	1936	17,888	674,076	21,375
	>2500	12,173	5702	26,789	572,169	18,143
	>5000	19,756	11,373	25,315	493,914	15,662
River slope (km/km)	>30	0.00096	0.00017	0.00421		
	>100	0.00049	0.00009	0.00423		
	>500	0.00015	0.00005	0.00044		
	>1000	0.00017	0.00005	0.00057		
	>2500	0.00008	0.00004	0.00016		
	>5000	0.00005	0.00003	0.00005		
Particle size (mm)	>30	5.5	0.3	42		
	>100	2.4	0.2	18		
	>500	1.6	0.1	8.0		
	>1000	2.0	0.1	10		
	>2500	0.4	0.1	1		
	>5000	0.3	0.08	0.8		
Susp. sediment (kg/s)	>30	321	20	3629	665,035	16,636[a]
	>100	672	72	5422	617,795	15,146[a]
	>500	2408	367	10,951	525,106	12,223[a]
	>1000	4261	968	14,924	485,830	10,984[a]
	>2500	9337	2371	22,393	438,864	9,503[a]
	>5000	15,866	4402	29,389	396,650	8,172[a]
SBM (kg/s)	>30	39	16	119	81,348	2,565
	>100	60	27	145	55,823	1,760
	>500	144	75	270	31,464	992
	>1000	220	106	353	25,189	794
	>2500	365	184	452	17,193	542
	>5000	529	416	565	13,228	417
Bedload (kg/s)	>30	17	6	41	36,302	1,145
	>100	22	8	52	20,976	661
	>500	42	16	89	9327	294
	>1000	66	30	118	7583	239
	>2500	109	56	150	5158	163
	>5000	140	75	178	3507	111
Washload (kg/s)	>30	291	7	3559	603,128	14,683[a]
	>100	619	40	5319	569,688	13,629[a]
	>500	2273	293	10,755	495,685	11,295[a]
	>1000	4328	834	14,668	461,493	10,217[a]
	>2500	8974	2108	22,038	421,779	8,964[a]
	>5000	15,340	3959	28,955	383,521	7,758[a]

Table 2
Continued

	Outlet filter (m^3/s)	Mean	Median	Standard deviation	Sum (m^3/s) or (kg/s)	Sum (km^3/y) or (MT/y)
Total sediment (kg/s)	>30	339	34	3648	701,337	17,780[a]
	>100	695	92	5449	638,772	15,807[a]
	>500	2451	388	11,003	534,434	12,517[a]
	>1000	4328	1003	14,991	493,414	11,223[a]
	>2500	9447	2500	22,483	444,023	9,666[a]
	>5000	16,006	4481	29,505	400,157	8,282[a]
Bedload proportion (%)	>30	32	22	28		6.4[a]
	>100	21	11	23		4.1[a]
	>500	11	3.6	17		2.3[a]
	>1000	9	3.2	15		2.1[a]
	>2500	5.3	1.9	9		1.6[a]
	>5000	4.4	1.2	9.7		1.3[a]
Bedload/suspended	>30	1.1	0.3	2.0		0.069[a]
	>100	0.5	0.1	0.9		0.044[a]
	>500	0.2	0.03	0.48		0.024[a]
	>1000	0.1	0.03	0.44		0.022[a]
	>2500	0.07	0.02	0.14		0.017[a]
	>5000	0.06	0.01	0.16		0.014[a]

Note. See Figure 6 caption for information about the number of outlets and landmass representation of each bracket. Bedload proportion Sum was calculated from bedload and total sediment Sum values.
[a]Values that are affected by adjustment of the suspended sediment values for the Amazon and Ganges-Brahmaputra Rivers.

3.5. Longitudinal Profiles

Spatial dynamics and trends along longitudinal profiles are analyzed for three rivers:

1. Mississippi/Missouri (Figure 8) - ~4,700 km north to south flow, covering over 10° latitude with substantial anthropogenic modification including large dams and long reservoirs.
2. Lena/Vitim (Figure 9) - ~4,500 km south to north flow, covering over 20° latitude (50° −70°), limited in-stream modifications, complex topographic profile.
3. Amazon/Marañón (Figure 10) - ~4,300 km west to east flow, minimal latitudinal range, and in-stream modifications.

The Mississippi/Missouri profile shows a sharp increase in Q_s from headwater to the coast, ranging ~5 orders of magnitude, and primarily driven by water discharge. Q_s fluctuate in response to damming (sharp drops, e.g., Canyon Ferry dam in km 350; Figure 8) and to tributary confluences (steep rise; Ohio River at km 3,400). Bedload has a comparatively smaller range, ~2 orders of magnitude, with a weak increasing trend downstream, and considerable fluctuations driven primarily by changes in river slope (Figures 8b and 8c). The Q_b proportion has a distinct logarithmic decay shape. River slope explains 80% of the variability in bedload spatial dynamics (Figure 8d) and, in conjunction with Q_s fluctuations due to dam trapping, can be inversely proportional to Q_s. Dams have contrasting effects on bedload proportion. By reducing Q_s, dams lead to an increase in bedload proportion (see two highlighted regions in the model of Figure 8) as the model Q_b equation is transport limited and thus does not account for potential reduction in bed material availability downstream of dams. However, large reservoirs reduce surface slope of rivers (DEMs record water rather than bed elevation), and this translates to a lower Q_b (most up and downstream highlighted regions in Figure 8). The overall impact of these two effects depends on the degree to which reservoir water slope is captured in the river slope data layer and the length of the reservoir. In WBMsed, sediment trapping behind dams is calculated at the dam location and thus, in long reservoirs, the decrease in Q_s will be predicted considerably downstream from the reservoir intake (where

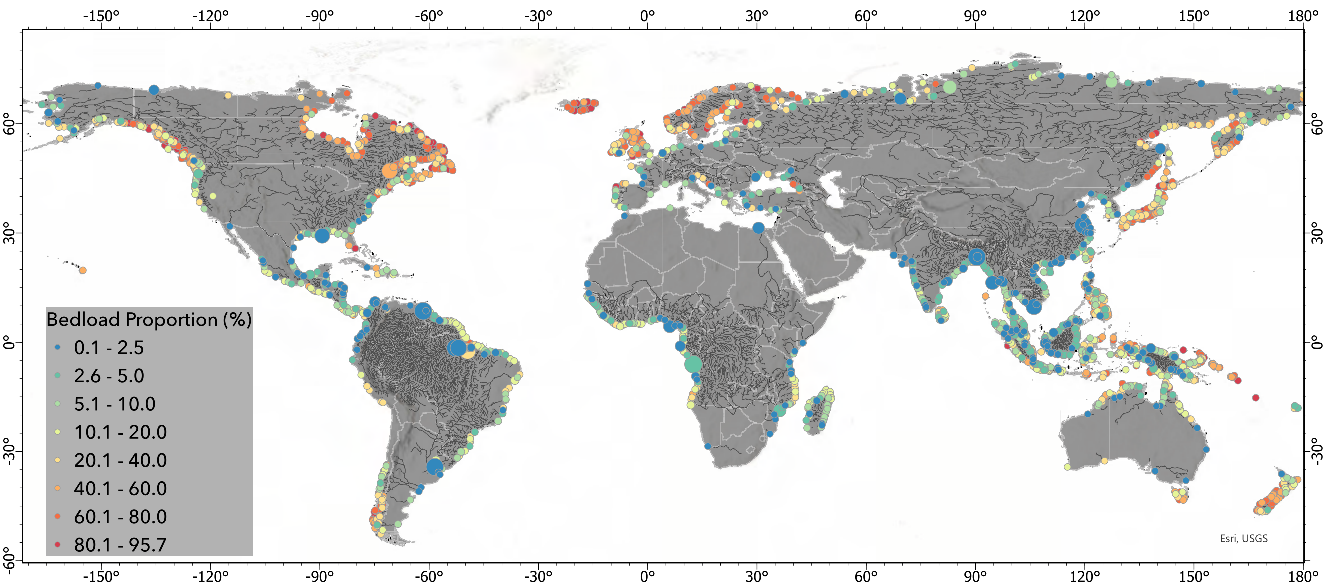

Figure 7. Bedload proportion (Q_b/Q_t) in 2,067 river outlets. The size of the icon represents river discharge.

sedimentation commences). This spatial mismatch is most clearly observed in the most downstream highlighted region in Figure 8, where the ~200 km long Lake Frances results in a considerable drop in river slope and bedload, but its impact on Q_s is only predicted downstream of the dam. Immediately upstream and downstream of Lake Frances are two sections of high bedload proportion, driven by high river slope values and a drop in Q_s due to the dams.

Except for these dam/reservoir-driven fluctuations, bedload proportion is very low for much of the river flow length (less than 5% after km 750). In the lower Mississippi (the most downstream 750 km or so), the bedload proportion is around 1%, driven by the very low river slope and very high Q_s. Bedload for the lower Mississippi is underpredicted compared to observations reported by Nittrouer et al. (2008), ~20 versus ~70 kg/s (hollow red star in Figures 8a and 8b) and Q_s is overpredicted compared to observations at the USGS Thebes, IL gage site (observed 2,550 kg/s; predicted 3,827 kg/s) ~1,500 km upstream of the coast (green star in Figures 8a and 8b). This suggests that bedload proportion is underpredicted in the lower Mississippi River.

The Lena/Vitim longitudinal profile of Q_s shows a relatively steady increase from headwater to the coast (2+ orders of magnitude) and a fluctuating Q_b, driven by river slope, with a general downstream increasing trend (Figures 9b and 9c). The bedload proportion along the Vitim River (flow length 950–1,100 km; blue highlight in Figure 9) sharply increases as the river flows through the Kodar Mountain Range in a relatively narrow valley with high slopes. The lowered Q_s across this narrow valley is an artifact of how upstream relief is calculated in WBMsed, particularly in narrow valleys where the coarse grid-cell can capture the surrounding, rather than the river, topography. Another zone of higher bedload proportion occurs in the middle of the profile (2,300–2,750 km; green highlight Figure 9) wherein river slope and Q_b are elevated. This section of the Lena River, downstream of the confluence with the Olekma River, is narrower and straight flowing with nearly no meandering and braiding. Downstream of this section, the river widens and bedload is likely sequestered, coinciding with lower Q_b predictions.

The coastal section of the Lena River has a predicted Q_b of ~200 kg/s (6 Mt/y), driven by high river slope values (Figure 9c). Q_b is underpredicted compared to a reported value of 14.9 Mt/y; Q_s is overpredicted with 75 Mt/y predicted versus 12–22 Mt/y observed (Holmes et al., 2002), though these observations (pre-1990) do not match the timeframe of the model simulations (1990–2019). As a result, the bedload proportion (~10%) on the lower Lena is likely considerably underpredicted. Babiński (2005), using several observation references, reported bedload proportion of 43% (Q_b = 17.45 Mt/y, Q_s = 22.6 Mt/y). Model predictions for the Lena River are particularly challenging given its extreme flow regime. Similar to other arctic rivers, the Lena is frozen with very low discharge for much of the year, with spring flooding (from near 0 to 120,000 m^3/s in a few days) and

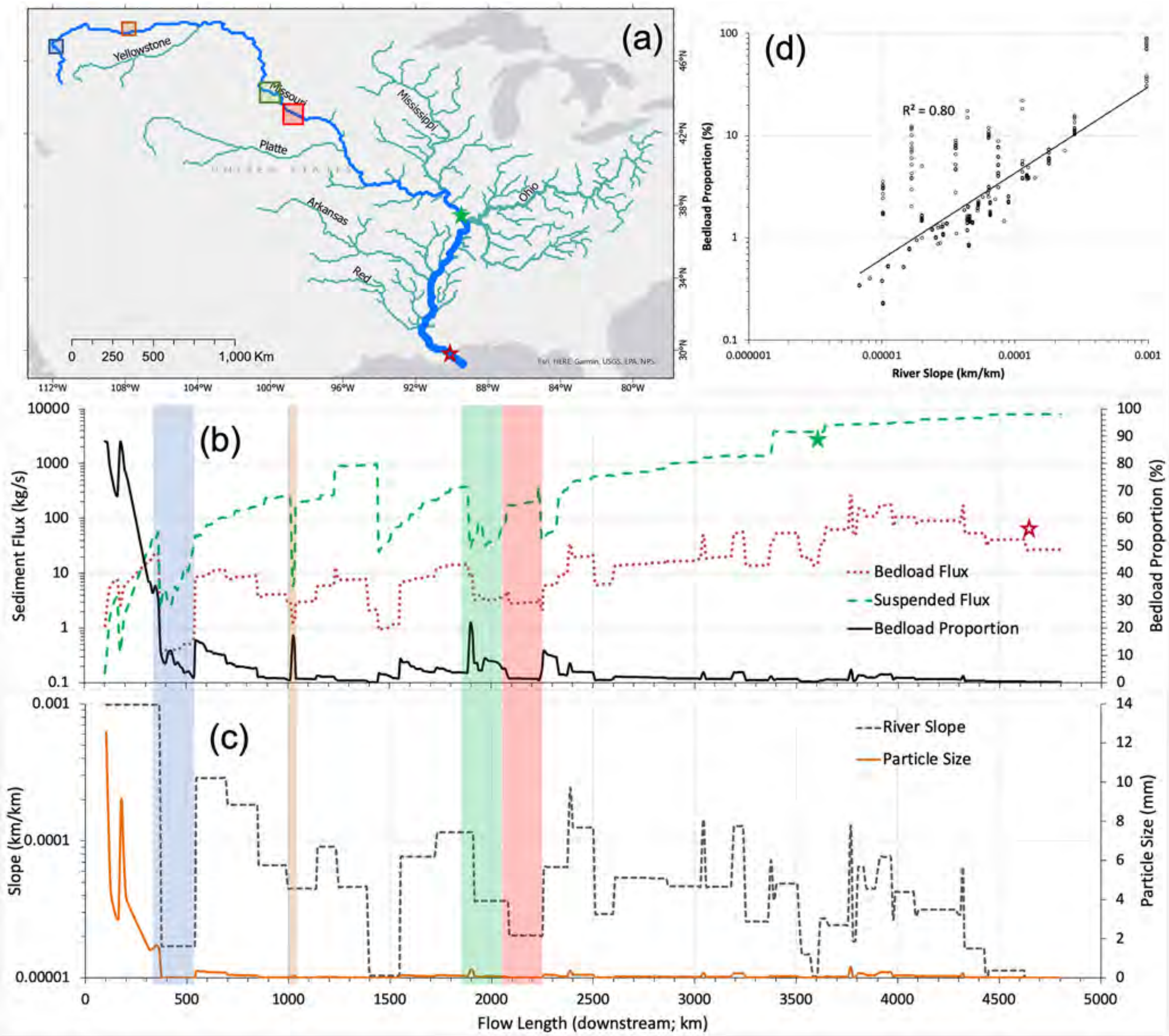

Figure 8. Mississippi/Missouri longitudinal profile (a) map, (b) bedload (kg/s), suspended load (kg/s) and bedload proportion (%), (c) river slope (−) and average bed-material grain size (mm), and (d) relationship between river slope (−) and bedload proportion (%). Colored bars on panels (b and c) correspond to boxes in panel (a). Green star (in panels (a and b)) is observed Q_s from gage site USGS 07022000 Mississippi River at Thebes, IL (2550 kg/s); Hollow red star (in panels (a and b)) is observed bedload from Nittrouer et al. (2008).

moderate flows in the summer (~20,000 m^3/s; Rachold et al., 1996). The very energetic annual spring floods were speculated to yield Q_b that exceeds Q_s (Are & Reimnitz, 2000).

The Amazon/Marañón River Q_s longitudinal profile increases downstream by over three orders of magnitude (Figure 10b). The Q_b profile shows more localized fluctuations with a very slight increasing trend downstream. Localized spikes and drops in bedload are driven by river slope (Figures 10c and 10d). The balancing effects of discharge, particle size, and river slope on Q_b are most clearly seen in this profile; slope decreases considerably downstream (~3 orders of magnitudes), while Q_b remains relatively consistent. Particle size decreases from ~6 mm in the upstream reaches to <0.2 mm downstream of the 600 km mark in Figure 8c (see also Figure 3). The 600 km mark is the transition from the Marañón's high altitude Andean valley section to the lower floodplains (Figure 10c). Bedload proportion drops dramatically from >30% upstream to <5% downstream of the Marañón's altitude transition. In the lower Amazon River, bedload proportion is very low (~1%), consistent with reported

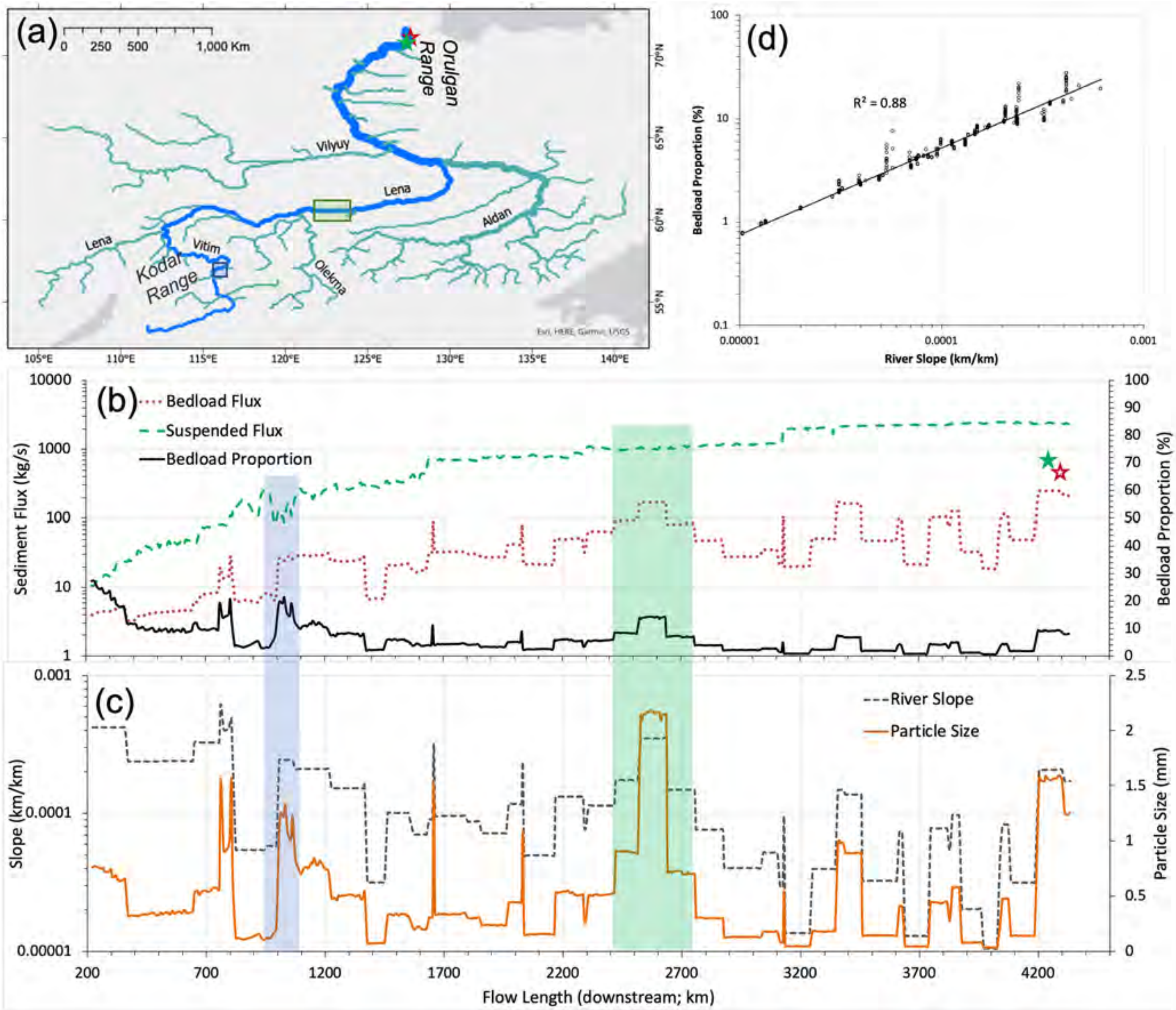

Figure 9. Lena/Vitim longitudinal profile (a) map, (b) bedload (kg/s), suspended load (kg/s) and bedload proportion (%), (c) river slope (−) and size-average bed-material grain size (mm), and (d) relationship between river slope (−) and bedload proportion (%). Colored bars on panels (b and c) correspond to boxes in panel (a). Green star (in panels (a and b)) is the average of reported SSF range at Kyusyr (11.8–21 Mt/yr; Are & Reimnitz, 2000); Hollow red star (in panels (a and b)) is observed bedload at Kusur GS reported by Fofonova et al. (2018).

estimates (Babiński, 2005). Bedload proportion is, however, likely underpredicted due to considerable overprediction of Q_s by the model (green star in Figure 10b).

Comparison of normalized elevation and bedload proportion for the three longitudinal profiles (Figure 11) offers several insights. Away from the headwaters, bedload proportion drops dramatically by 80%, 70%, and 80% within 10% of the downstream flow length (0.1 in Figure 11 *x*-axis) for the Mississippi/Missouri, Lena/Vitim, and Amazon/Marañón, respectively. The Missouri River shows considerable variability in bedload proportion due to mainstem river dams. Further downstream, the bedload proportion of the Mississippi/Missouri is quite similar to the Amazon/Marañón, with very low values. The Lena/Vitim, while having an elevation profile similar (albeit more complex) to the Mississippi/Missouri, has a different bedload proportion profile. The Amazon/Marañón is unique in that its bedload proportion profile closely aligns with its elevation profile. This is attributed to the low anthropogenic modification, and its relatively homogenous topography, climate, and inter-and intra-annual flow

10.1029/2021WR031583

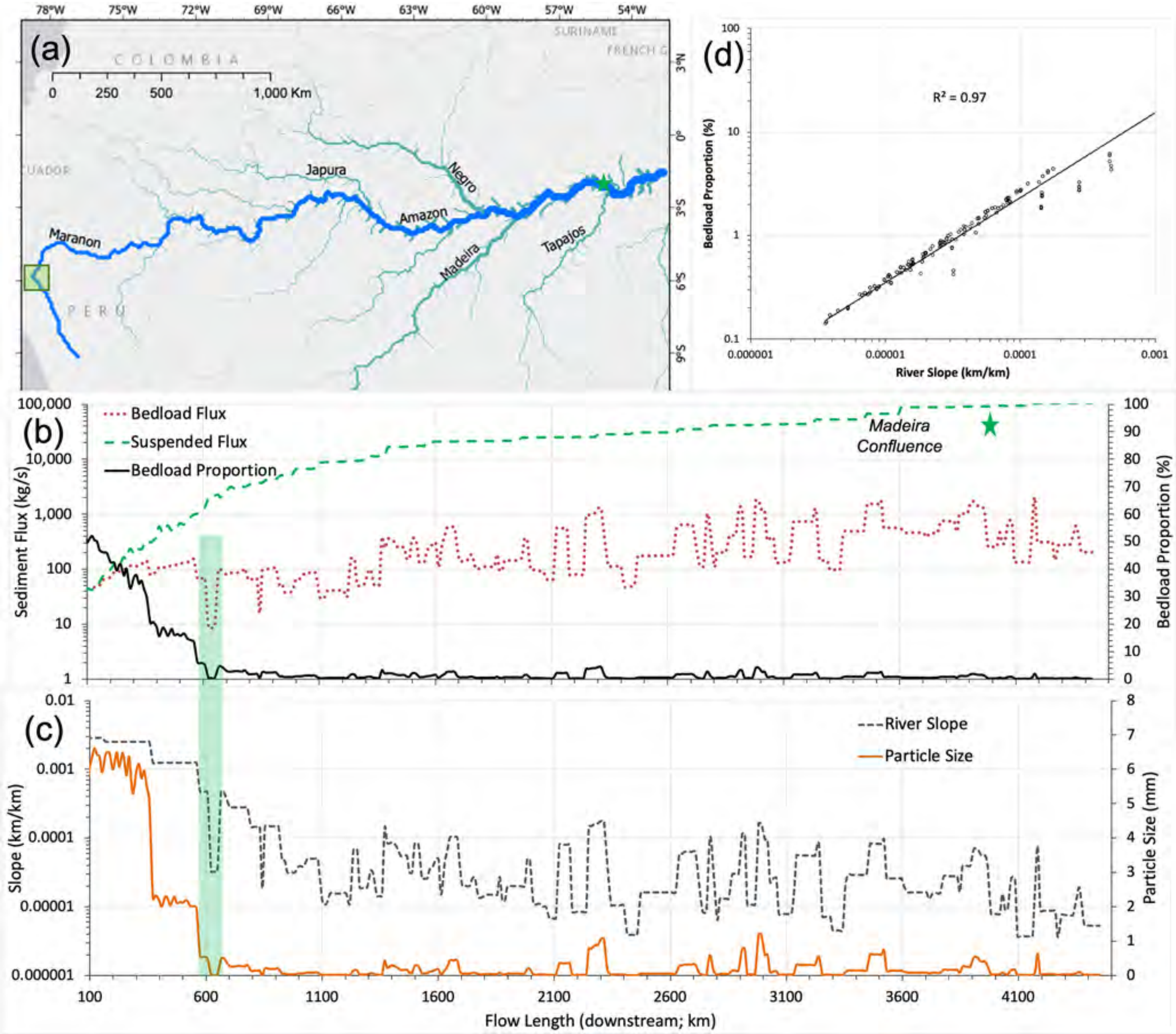

Figure 10. Amazon/Marañón longitudinal profile (a) map, (b) bedload (kg/s), suspended load (kg/s) and bedload proportion (%), (c) river slope (−) and size-average bed-material grain size (mm), and (d) relationship between river slope (−) and bedload proportion (%). Colored bar on panels (b and c) correspond to boxes in panel (a). Green star (in panels (a and b)) is a range of observed SSF at Óbidos summarized in Montanher et al. (2018).

regime. The Lena/Vitim has very low anthropogenic modifications but extreme seasonal streamflow fluctuations, complex topography, and considerable climatic gradient from headwater to the coast.

This comparison highlights the impacts of anthropogenic modifications, topographic characteristics, climatic gradient/heterogeneity, and flow regime on longitudinal variability in bedload. Q_b dynamics is considerably more complex than Q_s profiles, undermining the assertion that Q_b can be deducted/derived from Q_s alone. Our analysis highlights the need for increased accuracy for two key Q_b driving parameters: river slope and particle size.

4. Discussion and Conclusions

New bedload (Q_b) and suspended bed material flux (Q_{sbm}) modules are introduced within the global-scale WBMsed hydrogeomorphic model. Global-scale modeling of bedload is enabled by simplified equation parameterizations proposed by Lammers and Bledsoe (2018) and Syvitski et al. (2019). The analysis presented here is

10.1029/2021WR031583

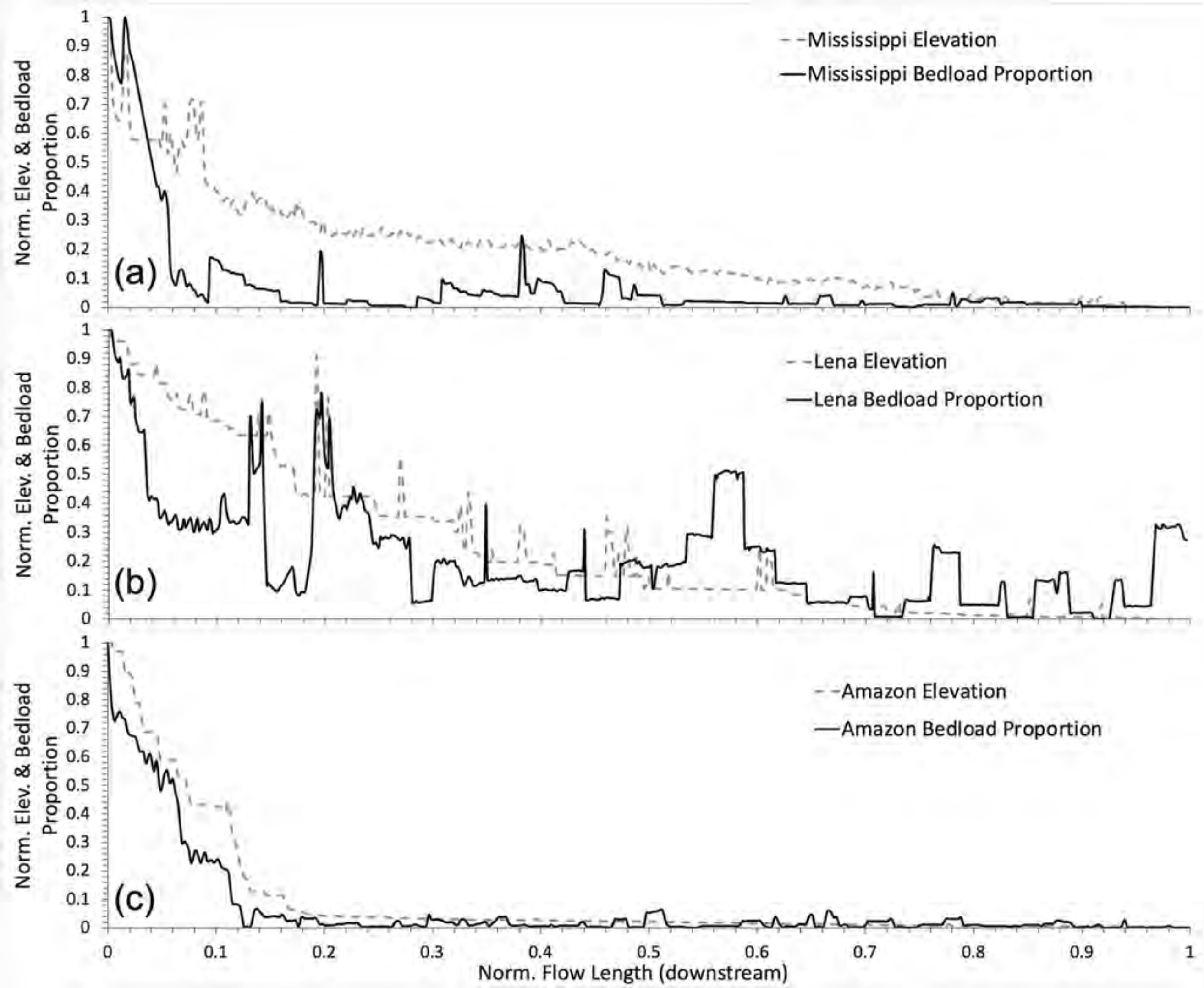

Figure 11. Normalized [0,1] bedload proportion and elevation profiles along a normalized longitudinal profile for (a) Mississippi/Missouri, (b) Lena/Vitim, and (c) Amazon/Marañón.

based on long-term average (1990–2019) model predictions at 6 arc-minute spatial resolution for grid cells with average discharge larger than 30 m^3/s.

WBMsed can well capture average discharge, suspended load (Q_s), and Q_b. The comparison against observed Q_b should not be taken at face value as bedload observations are determined typically from near-instantaneous measurements (e.g., Helley-Smith sampler) or as an average across short intervals (e.g., bedload traps or sonar mapping) (Fekete et al., 2021). The data set used here was mostly from rivers in the US and observed values with limited temporal representation were compared to long-term average model predictions (1990–2019). Due to its time-consuming and expensive nature, long-term and continuous bedload monitoring is rare, especially for large rivers. Some model bedload parameters, primarily river slope, and particle size are spatially variable and can result in noisy longitudinal profiles, complicating comparison to observations in discrete locations. There remains a severe scarcity of bedload evaluation data at the global scale, hindering a robust validation analysis.

Bedload predictions are highly sensitive to discharge, slope, channel width, and riverbed particle size. In this study, an improved global river slope data set and a novel particle size calculation equation are used. However, the grain size predictions are ideal or generalized and do not include local lithology, or geological lags from prior climates or deglacial conditions and Earth's ability to return to an equilibrium state. Paraglacial conditions remain in place for many parts of the Arctic (Forbes & Syvitski, 1995). Recent advancements in global-scale DEM resolution, accuracy, and processing tools (e.g., Google Earth Engine) can be utilized for improving river slope calculations. Emerging datasets and analysis techniques can also be used to improve particle size predictions. Abeshu et al. (2021), for example, present a very promising particle size database for the US based on extensive data mining and machine learning analysis.

The Q_b model is transport-limited, meaning that it assumes there is unlimited bed material to be transported when local specific stream powers exceed the critical stream powers ($\omega > \omega_c$ in Equation 1). While this is a reasonable assumption in many (perhaps most) large rivers, particularly for averaged predictions at relatively coarse resolution, it merits further analysis. The model of Hatono and Yoshimura (2020) simulates riverbed sediment deposition, erosion, and transport and is likely the most mechanistically explicit global scale fluvial sediment model. Their analysis shows that the model results are not sensitive to riverbed dynamics which raises the question of whether small-scale transport processes can be realistically be simulated at kilometers-scale resolution. We assert that advancement toward greater mechanistic representation is warranted and, indeed, needed in order to better predict fluvial dynamics. As demonstrated in the present paper, alleviating uncertainty in input data, and expanding observational data (e.g., using sedimentation in lakes and reservoirs) are key for further advancements.

Model predicted Q_b is spatially heterogenous both between and within basins. In some river basins, high Q_b values are in the headwater and coastal reaches, while others show a general downstream-increasing trend. The heterogeneity in intra-basin Q_b dynamics is a function of the relative changes in river slope and discharge downstream, with general decreasing and increasing trends respectively. The topographic and hydrological longitudinal profiles of rivers are shown to be the key driver of Q_b longitudinal trends with fluctuations in slope controlling its more local dynamics. The proportion of bedload out of the total particulate flux is very low in most downstream reaches and high in smaller rivers and high latitude rivers. The average bedload proportion for all analyzed grid-cells (unweighted) is 24% but with considerable variability.

We offer an estimate of average modern sediment discharge to global oceans. While estimated water discharge values closely match recently published values, our sediment flux values exceed past assessments. We assert that our results, after adjustment for the Amazon and Ganges-Brahmaputra rivers, are robust as (a) the model Q and Q_s predictions well correspond to observations, and (b) our analysis is more extensive than past studies in terms of the number of rivers analyzed. Furthermore, the fluxes may actually be conservative as the river outlets analyzed represents just ∼70% of Earth's landmass, excludes Greenland, and the model underpredicts Q. Water discharge to global oceans (1990–2019) is predicted to be 30,579 km^3/y, over half of which is from Earth's 25 largest rivers. Q_s to global oceans is predicted to be 16,636 Mt/y, nearly 50% of which is from the 25 largest rivers. Washload ($Q_s - Q_{sbm}$) to global oceans is predicted to be 14,683 MT/y with the 25 largest rivers contributing over 50%. Q_b to global oceans is predicted to be 1,145 MT/y, only ∼10% of which is from the 25 largest rivers. Total sediment flux to global oceans is predicted to be 17,780 Mt/y (17 Gt/y), 46% of which is from the 25 largest rivers.

Analysis of longitudinal profiles of the Amazon/Marañón, Mississippi/Missouri, and Lena/Vitim rivers, shows that spatial dynamics in bedload are strongly controlled by river slope and thus very sensitive to noise in its input data set. A comparison between the three profiles shows that anthropogenic modifications (dams and reservoirs) and topographic features (ridges, physiographic province transitions) have localized and downstream-propagating impacts on bedload and bedload proportion respectfully. Climatic gradient and flow regime also influence trends in bedload (and thus Q_b proportion). This analysis further demonstrates the complexity of intra-basin bedload dynamics and thus the futility in its estimation based on Q or Q_s alone at these scales. The results also demonstrate the need to enhance the representation of riverbed particle size and river slope, as it was found to be the primary source of uncertainty in the model predictions.

Perhaps the larger concern comes from our modeling capability versus the speed at which humans are altering our planet. Sand and gravel mining from coasts and rivers have reached ∼40 Gt/y (Peduzzi, 2014), more than the total fluvial sediment load. Fluvial sand, being more angular, is much preferred in concrete production compared with rounded particles found on many coastal beaches or desert dunes. As a consequence, riverbed mining is now global, greatly reducing fluvial bed-material transport. 55 Mt/y of aggregates are extracted from the lower Mekong (Bravard et al., 2013), an order of magnitude higher than the down-river transport of sand at 6.2 Mt/y, with riverbank and coastal erosion being the result (Bendixen et al., 2019; Hackney et al., 2020).

Data Availability Statement

The WBMsed model input data and model predictions are available on the lead-author's institute and lab servers. See https://sdml.ua.edu/datasets-2/ for more information. The WBMsed core model code is available on the CSDMS model repository https://csdms.colorado.edu/wiki/Model:WBMsed. The global maps presented in the figures are accsessable for interactive view on ArcGIS Online Map Viewer: https://arcg.is/1m5W4m0.

Acknowledgments
S. Cohen thanks the National Science Foundation Geography and Spatial Sciences Program for the initial funding of this project (Grant 1561082). H.-Y. Li acknowledges his support as part of the Energy Exascale Earth System Model (E3SM) project, funded by the US Department of Energy, Office of Science, Office of Biological and Environmental Research, via Lawrence Livermore National Laboratory (Contract B633822).

References

Abatzoglou, J. T., Dobrowski, S. Z., Parks, S. A., & Hegewisch, K. C. (2018). *Terraclimate, a high-resolution global dataset of monthly climate and climatic water balance from 1958-2015*. Scientific Data, 1–12.

Abeshu, G. W., Li, H.-Y., Zhu, Z., & Leung, L. R. (2021). Median bed-material sediment particle size across rivers in the contiguous U.S. *Earth System Science Data Discussions*, *14*(2), 929–942. https://doi.org/10.5194/essd-2021-201

Are, F., & Reimnitz, E. (2000). An overview of the Lena River Delta setting: Geology, tectonics, geomorphology, and hydrology. *Journal of Coastal Research*, *16*(4), 1083–1093. Retrieved from https://www.jstor.org/stable/4300125

Ashley, T. C., McElroy, B., Buscombe, D., Grams, P. E., & Kaplinski, M. (2020). Estimating bedload from suspended load and water discharge in sand bed rivers. *Water Resources Research*, *56*(2), e2019WR025883. https://doi.org/10.1029/2019wr025883

Babiński, Z. (2005). *The relationship between suspended and bed load transport in river channels*. IAHS Publ. W: Sediment Budgets 1.

Bagnold, R. A. (1966). An approach to the sediment transport problem from general physics. *U. S. Geological Survey Professional Paper*, *422*, 1–37.

Bendixen, M., Best, J., Hackney, C., & Iversen, L. L. (2019). Time is running out for sand. *Nature*, *571*(7763), 29–31. https://doi.org/10.1038/d41586-019-02042-4

Best, J. (2019). Anthropogenic stresses on the world's big rivers. *Nature Geoscience*, *12*(1), 7–21. https://doi.org/10.1038/s41561-018-0262-x

Bravard, J. P., Goichot, M., & Gaillot, S. (2013). Geography of sand and gravel mining in the Lower Mekong River. First survey and impact assessment. *EchoGéo*, *26*. https://doi.org/10.4000/echogeo.13659

Cohen, S., Kettner, A. J., & Syvitski, J. P. M. (2014). Global suspended sediment and water discharge dynamics between 1960 and 2010: Continental trends and intra-basin sensitivity. *Global and Planetary Change*, *115*, 44–58. https://doi.org/10.1016/j.gloplacha.2014.01.011

Cohen, S., Kettner, A. J., Syvitski, J. P. M., & Fekete, B. M. (2013). WBMsed, a distributed global-scale riverine sediment flux model: Model description and validation. *Computers & Geosciences*, *53*, 80–93. https://doi.org/10.1016/j.cageo.2011.08.011

Cohen, S., Wan, T., Islam, M. T., & Syvitski, J. P. M. (2018). Global River slope: A new geospatial dataset and global-scale analysis. *Journal of Hydrology*, *563*, 1057–1067. https://doi.org/10.1016/j.jhydrol.2018.06.066

Coulthard, T. J., Neal, J. C., Bates, P. D., Ramirez, J., de Almeida, G. A. M., & Hancock, G. R. (2013). Integrating the LISFLOOD-FP 2D hydrodynamic model with the CAESAR model: Implications for modelling landscape evo-lution. *Earth Surface Processes and Landforms*, *38*, 1897–1906. https://doi.org/10.1002/esp.3478

Dunn, F. E., Darby, S. E., Nicholls, R. J., Cohen, S., Zarfl, C., & Fekete, B. M. (2019). Projections of declining fluvial sediment delivery to major deltas worldwide in response to climate change and anthropogenic stress. *Environmental Research Letters*, *14*(8), 084034. https://doi.org/10.1088/1748-9326/ab304e

Dunn, F. E., Nicholls, R. J., Darby, S. E., Cohen, S., Zarfl, C., & Fekete, B. M. (2018). Projections of historical and 21st century fluvial sediment delivery to the Ganges-Brahmaputra-Meghna, Mahanadi, and Volta deltas. *Science of The Total Environment*, *642*, 105–116. https://doi.org/10.1016/j.scitotenv.2018.06.006

Dunne, K. B., & Jerolmack, D. J. (2018). Evidence of, and a proposed explanation for, bimodal transport states in alluvial rivers. *Earth Surface Dynamics*, *6*(3), 583–594. https://doi.org/10.5194/esurf-6-583-2018

Engelund, F., & Hansen, E. (1967). A monograph on sediment transport in alluvial streams. *Monografia*.

Fekete, B. M., Andreu, A., Argent, R., Avellán, T., Birkett, C., Caucci, S., et al. (2021). Observations, monitoring and data management. In J. J. Bogardi, J. Gupta, K. D. W. Nandalal, L. Salamé, R. R. P. van Nooijen, N. Kumar, et al. (Eds.), *Handbook of water Resources management*: *Discourses, concepts and examples* (pp. 385–442).

Fofonova, V., Zhilyaev, I., Kraineva, M., Iakshina, D., Tananaev, N., Volkova, N., et al. (2018). Features of the water temperature long-term observations on the Lena River at basin outlet. *Polarforschung*, *87*(2), 135–150. https://doi.org/10.2312/polarforschung.87.2.135

Forbes, D., & Syvitski, J. P. M. (1995). Paraglacial coasts. In C. Woodruffe & R. W. G. Carter (Eds.), *Coastal evolution* (pp. 373–424). Cambridge University of Press. Chapter 10.

Gomez, B. (1991). Bedload transport. *Earth-Science Reviews*, *31*(2), 89–132.

Hackney, C. R., Darby, S. E., Parsons, D. R., Leyland, J., Best, J. L., Aalto, R., et al. (2020). River bank instability from unsustainable sand mining in the lower Mekong River. *Nature Sustainability*, *3*, 217–225. https://doi.org/10.1038/s41893-019-0455-3

Hatono, M., & Yoshimura, K. (2020). Development of a global sediment dynamics model. *Progress in Earth and Planetary Science*, *7*, 59. https://doi.org/10.1186/s40645-020-00368-6

Holmes, R. M., McClelland, J. W., Peterson, B. J., Shiklomanov, I. A., Shiklomanov, A. I., Zhulidov, A. V., et al. (2002). A circumpolar perspective on fluvial sediment flux to the Arctic Ocean. *Global Biogeochemical Cycles*, *16*(4), 45–1. https://doi.org/10.1029/2001GB001849

Islam, M. T. (2018). *Global scale bedload flux modeling*. The University of Alabama.

Kabir, M. A., Dutta, D., Hironaka, S., & Pang, A. (2012). Analysis of bed load equations and river bed level variations using basin-scale process-based modelling approach. *Water Resources Management*, *26*(5), 1143–1163. https://doi.org/10.1007/s11269-011-9951-6

Kalnay, E., Kanamitsu, M., Kistler, R., Collins, W., Deaven, D., Gandin, L., et al. (1996). *The NCEP/NCAR 40-year reanalysis project* (Vol. 77). Bulletin of the American Meteorological society

Kettner, A. J., & Syvitski, J. P. M. (2008). HydroTrend v.3.0: A climate-driven hydrological transport model that simulates discharge and sediment load leaving a River system. *Computers & Geosciences*, *34*(10), 1170–1183. https://doi.org/10.1016/j.cageo.2008.02.008

Kistler, R., Kalnay, E., Collins, W., Saha, S., White, G., Woollen, J., et al. (2001). The NCEP–NCAR 50-year reanalysis: Monthly means CD-ROM and documentation. *Bulletin of the American Meteorological Society*, *82*(2), 247–268. https://doi.org/10.1175/1520-0477(2001)082<0247:tnnyrm>2.3.co;2

Lammers, R. W., & Bledsoe, B. P. (2018). Parsimonious sediment transport equations based on Bagnold's stream power approach. *Earth Surface Processes and Landforms*, *43*(1), 242–258. https://doi.org/10.1002/esp.4237

Lehner, B., Reidy Liermann, C., Revenga, C., Vörösmarty, C., Fekete, B., Crouzet, P., et al. (2011). High-resolution mapping of the world's reservoirs and dams for sustainable river-flow management. *Frontiers in Ecology and the Environment*, *9*(9), 494–502. https://doi.org/10.1890/100125

Lehner, B., Verdin, K. L., & Jarvis, A. (2008). New global hydrography derived from spaceborne elevation data. *AGU EOS Transactions*, *89*(10), 93–94. https://doi.org/10.1029/2008eo100001

Li, H.-Y., Tan, Z., Ma, H., Zhu, Z., Abeshu, G. W., Zhu, S., et al. (2022). A new large-scale suspended sediment model and its application over the United States. *Hydrology and Earth System Sciences*, *26*, 665–688. https://doi.org/10.5194/hess-26-665-2022

Li, L., Ni, J., Chang, F., Yue, Y., Frolova, N., Magritsky, D., et al. (2020). Global trends in water and sediment fluxes of the world's large rivers. *Science Bulletin*, *65*(1), 62–69. https://doi.org/10.1016/j.scib.2019.09.012

Lin, P., Pan, M., Allen, G. H., de Moraes Frasson, R. P., Zeng, Z., Yamazaki, D., & Wood, E. F. (2020). Global estimates of reach-level bankfull river width leveraging big data geospatial analysis. *Geophysical Research Letters*, *47*, e2019GL086405. https://doi.org/10.1029/2019GL086405

Ma, H., Nittrouer, J. A., Naito, K., Fu, X., Zhang, Y., Moodie, A. J., et al. (2017). The exceptional sediment load of fine-grained dispersal systems: Example of the Yellow River, China. *Science Advances*, *3*(5), e1603114. https://doi.org/10.1126/sciadv.1603114

McCutcheon, S. C., Martin, J. L., & Barnwell, T. O., Jr. (1993). Chapter 11: Water quality. In D. R. Maidment (Ed.), *Handbook of hydrology*. McGraw Hill.

McKay, L., Bondelid, T., Dewald, T., Johnston, J., Moore, R., & Rea, A. (2012). NHDPlus version 2: User guide.

Meade, R. H., Yuzyk, T. R., & Day, T. J. (1990). Movement and storage of sediment in rivers of the United States and Canada. In M. G. Wolman, & H. C. Riggs (Eds.), *Surface water hydrology—The geology of north America: Boulder, colo* (pp. 255–280). Geological Society of America.

Meyer-Peter, E., & Müller, R. (1948). *Formulas for bedload transport*. In *Paper presented at the 2nd meeting of the international association of hydraulic structures research*.

Miara, A., Vörösmarty, C. J., Macknick, J. E., Tidwell, V. C., Fekete, B., Corsi, F., & Newmark, R. (2018). Thermal pollution impacts on rivers and power supply in the Mississippi River watershed. *Environmental Research Letters*, *13*, 034033. https://doi.org/10.1088/1748-9326/aaac85

Milliman, J. D., & Farnsworth, K. L. (2011). *river discharge to the coastal ocean: A global synthesis*. Cambridge University Press.

Montanher, O. C., Novo, E. M. L. D. M., & Souza Filho, E. E. D. (2018). Temporal trend of the suspended sediment transport of the Amazon River (1984–2016). *Hydrological Sciences Journal*, *63*(13–14), 1901–1912. https://doi.org/10.1080/02626667.2018.1546387

Moragoda, N., & Cohen, S. (2020). Climate-induced trends in global riverine water discharge and suspended sediment dynamics in the 21st century. *Global and Planetary Change*, *191*, 103199. https://doi.org/10.1016/j.gloplacha.2020.103199

Morehead, M. D., Syvitski, J. P. M., Hutton, E. W. H., & Peckham, S. D. (2003). Modeling the inter-annual and intra-annual variability in the flux of sediment in ungauged river basins. *Global and Planetary Change*, *39*(1/2), 95–110. https://doi.org/10.1016/S0921-8181(03)00019-5

Nittrouer, J. A., Allison, M. A., & Campanella, R. (2008). Bedform transport rates for the lowermost Mississippi River. *Journal of Geophysical Research*, *113*(F3), F03004. https://doi.org/10.1029/2007jf000795

Overeem, I., Hudson, B., Syvitski, J., Mikkelsen, A. B., Hasholt, B., van den Broeke, M. R., et al. (2017). Substantial export of suspended sediment to the global oceans from glacial erosion in Greenland. *Nature Geoscience*, *10*, 859–863. https://doi.org/10.1038/ngeo3046

Parker, G. (1990). Surface-based bedload transport relation for gravel rivers. *Journal of Hydraulic Research*, *28*(4), 417–436. https://doi.org/10.1080/00221689009499058

Peduzzi, P. (2014). Sand, rarer than one thinks. *Environmental Development*, *11*, 208–218. https://doi.org/10.1016/j.envdev.2014.04.001

Rachold, V., Alabyan, A., Hubberten, H.-W., Korotaev, V. N., & Zaitsev, A. A. (1996). Sediment transport to the Laptev sea–hydrology and geochemistry of the Lena River. *Polar Research*, *15*(2), 183–196. https://doi.org/10.3402/polar.v15i2.6646

Rahman, M., Dustegir, M., Karim, R., Haque, A., Nicholls, R. J., Darby, S. E., et al. (2018). Recent sediment flux to the Ganges-Brahmaputra-Meghna delta system. *Science of the Total Environment*, *643*, 1054–1064. https://doi.org/10.1016/j.scitotenv.2018.06.147

Recking, A. (2019). BedloadWeb user manuel. https://doi.org/10.13140/RG.2.2.32856.34564/1

Schmitt, R. J., Bizzi, S., & Castelletti, A. (2016). Tracking multiple sediment cascades at the river network scale identifies controls and emerging patterns of sediment connectivity. *Water Resources Research*, *52*(5), 3941–3965. https://doi.org/10.1002/2015WR018097

Syvitski, J., Ángel, J. R., Saito, Y., Overeem, I., Vörösmarty, C. J., Wang, H., & Olago, D. (2022). Earth's sediment cycle during the Anthropocene. *Nature Reviews Earth & Environment*, *3*(3), 179–196. https://doi.org/10.1038/s43017-021-00253-w

Syvitski, J., Cohen, S., Miara, A., & Best, J. (2019). River temperature and the thermal-dynamic transport of sediment. *Global and Planetary Change*, *178*, 168–183. https://doi.org/10.1016/j.gloplacha.2019.04.011

Syvitski, J., & Milliman, J. D. (2007). Geology, geography, and humans battle for dominance over the delivery of sediment to the coastal ocean. *The Journal of Geology*, *115*, 1–19. https://doi.org/10.1086/509246

Syvitski, J., & Saito, Y. (2007). Morphodynamics of deltas under the influence of humans. *Global and Planetary Change*, *57*(3–4), 261–282.

Syvitski, J., Vörösmarty, C. J., Kettner, A. J., & Green, P. (2005). Impact of humans on the flux of terrestrial sediment to the global coastal ocean. *Science*, *308*(5720), 376–380. https://doi.org/10.1016/j.gloplacha.2006.12.001

Wisser, D., Frolking, S., Douglas, E., Fekete, B. M., Schuman, A. H., & Vörösmarty, C. J. (2010). The significance of local water resources captured in small reservoirs for crop production—A global-scale analysis. *Journal of Hydrology*, *384*, 264–275. https://doi.org/10.1016/j.jhydrol.2009.07.032

Wollheim, W. M., Vörösmarty, C. J., Bouwman, A. F., Green, P., Harrison, J., Linder, E., et al. (2008). Global N removal by freshwater aquatic systems using a spatially distributed, within-basin approach. *Global Biogeochemical Cycles*, *22*(2), GB2026. https://doi.org/10.1029/2007gb002963